A New Arrangement for the Anticancer Antibiotics Tallysomycin and Bleomycin When Bound to Zinc: An Assessment of Metal and Ligand Chirality by NMR and Molecular Dynamics

Antonia M. Calafat, Hoshik Won, and Luigi G. Marzilli*

Contribution from the Department of Chemistry, Emory University, Atlanta, Georgia 30322

Received September 27, 1996[⊗]

Abstract: Bleomycin A_2 ($BLMA_2$, a clinically used drug) and tallysomycin A (TLMA) are two closely related anticancer antibiotics activated by O_2 reaction with their Fe(II) complexes. Fe(II) can be modeled by Zn(II). Evidence obtained that the disaccharide and metal-binding domains of ZnTLMA and $ZnBLMA_2$ are superimposable includes the following very similar NMR features: the ^1H and ^{13}C NMR chemical shifts, the ^1H and ^{13}C chemical shift changes upon Zn(II) binding, and the NOESY spectra. We evaluated several ZnTLMA structural models with four and five ligating donor atoms from TLMA by using 2D NMR, NOESY back-calculation methods, and restrained molecular mechanics/molecular dynamics calculations. Our results are most consistent with ligation by five N donors, the β-aminoalanine (ALA) amines (NC2 and NC3), the pyrimidinylpropionamide (PRO) pyrimidine (NC10), and the β-hydroxyhistidine amide (NC12) and imidazole (NC29). Metal complexation to TLMA or $BLMA_2$ creates newly stable chiral centers (the metal and the ALA secondary amine, NC3); for the first time, an extensive analysis of the chirality of both centers has been performed. A cross-peak between a PRO H and a disaccharide mannose H is clearly present in the low mixing time NOESY spectrum of ZnTLMA and in the published spectrum of $ZnBLMA_2$. This cross-peak has led us to discover a novel square pyramid (sp) basket arrangement of the drug donor atoms, with PRO NC10 at the apex and *SS* chirality. A close variant, with donors adopting a trigonal bipyramidal (tbp) arrangement, gave results almost as satisfactory. Our findings raise interesting aspects relevant to drug activation. The literature suggests that the activated form is $HO_2Fe(III)BLMA_2$; the five N donors are in an *SS*-sp I arrangement, with the ALA primary amine (NC2) at the apex. If the Fe(II) form of the drugs had the *SS*-sp basket or *SS*-tbp arrangement, addition of O_2 could yield products with the drug in an *SS*-sp I arrangement. Models with *RR* chirality, such as proposed previously for $ZnBLMA_2$, are energetically unfavorable, cannot account for the NMR results, and cannot readily convert to the *SS*-sp I geometry. Unlike in *RR* models, the carbamoyl group of the mannose cannot bind to the metal in *SS* models. Instead, in our model the disaccharide covers the sixth binding site.

Introduction

Bleomycins (BLMs) are a group of glycopeptide antibiotics, with significant anticancer activity.[1] The closely related tallysomycins (TLMs)[2−4] contain an additional sugar, 4-amino-4,6-dideoxy-L-talose, and lack a methyl group in the valerate moiety. In the presence of redox-active metals and molecular oxygen, tallysomycin A (TLMA, Figure 1) induced DNA strand scission[5] with a different site/sequence specificity than BLMs.[6,7] BLMs also cleave RNA oxidatively.[7,8] Fe(II)BLM undergoes redox reactions with O_2 that generate the active species responsible for the anticancer activity of BLM. Although the exact arrangement of the BLM ligand is not known, recent electrospray mass spectrometry (EMS)[9] and X-ray absorption spectroscopy[10] studies suggest that the active species is a ferric hydroperoxide complex.

No crystal structure of a metal−BLM (M−BLM) complex is known. X-ray structures of Co[11] and Cu[12,13] bound to simple BLM analogs lacking some BLM moieties (e.g., sugar rings and the bithiazole tail) are known. Typically, five N donor atoms are arranged around the metal as in a square pyramid (sp). A Zn(II)BLM analog complex was recently shown to have a trigonal bipyramidal (tbp) geometry with a coordinated deprotonated amide.[14] The ligand used for Zn is very similar to BLM analogs that bind to other metals in an sp arrangement.[12]

[⊗] Abstract published in *Advance ACS Abstracts,* April 1, 1997.

(1) Umezawa, H.; Maeda, K.; Takeuchi, T.; Oakami, Y. *J. Antibiot., A* **1966**, *19*, 200−209.

(2) Kawaguchi, H.; Tsukiura, H.; Tomita, K.; Konishi, M.; Saito, K.; Kobaru, S.; Numata, K.; Fujisawa, K.; Miyaki, T.; Hatori, M.; Koshiyama, H. *J. Antibiot.* **1977**, *30*, 779−788.

(3) Konishi, M.; Saito, K.; Numata, K.; Tsuno, T.; Asama, K.; Tsukiura, H.; Naito, T.; Kawaguchi, H. *J. Antibiot.* **1977**, *30*, 789−805.

(4) Miyaki, T.; Tenmyo, O.; Numata, K.-i.; Matsumoto, K.; Yamamoto, H.; Nishiyama, Y.; Ohbayashi, M.; Imanishi, H.; Konishi, M.; Kawaguchi, H. *J. Antibiot.* **1981**, *34*, 658−664.

(5) Mirabelli, C. K.; Huang, C.-H.; Crooke, S. T. *Biochemistry* **1983**, *22*, 300−306 and references therein.

(6) Petering, D. H.; Mao, Q. K.; Li, W. B.; Derose, E.; Antholine, W. E. In *Metal Ions in Biological Systems*; Sigel, A., Sigel, H., Eds.; Marcel Dekker: New York, 1996; Vol. 33, pp 619−648.

(7) Kane, S. A.; Hecht, S. M. In *Progress in Nucleic Acid Research and Molecular Biology*; Cohn, W. E., Moldave, K., Eds.; Academic Press Inc.: San Diego, 1994; Vol. 49, pp 313−352.

(8) Battigello, J. M.; Cui, M.; Carter, B. J. In *Metal Ions in Biological Systems*; Sigel, A., Sigel, H., Eds.; Marcel Dekker: New York, 1996; Vol. 33, pp 593−617.

(9) Sam, J. W.; Tang, X. J.; Peisach, J. *J. Am. Chem. Soc.* **1994**, *116*, 5250−5256.

(10) Westre, T. E.; Loeb, K. E.; Zaleski, J. M.; Hedman, B.; Hodgson, K. O.; Solomon, E. I. *J. Am. Chem. Soc.* **1995**, *117*, 1309−1313.

(11) Farinas, E.; Tan, J. D.; Baidya, N.; Mascharak, P. K. *J. Am. Chem. Soc.* **1993**, *115*, 2996−2997 and references therein.

(12) Kimura, E.; Kurosaki, H.; Kurogi, Y.; Shionoya, M.; Shiro, M. *Inorg. Chem.* **1992**, *31*, 4314−4321 and references therein.

(13) Iitaka, Y.; Nakamura, H.; Nakatani, T.; Muraoka, Y.; Fujii, A.; Takita, T.; Umezawa, H. *J. Antibiot.* **1978**, *31*, 1070−1072.

(14) Kurosaki, H.; Hayashi, K.; Ishikawa, Y.; Goto, M. *Chem. Lett.* **1995**, 691−692.

S0002-7863(96)03392-6 CCC: $14.00

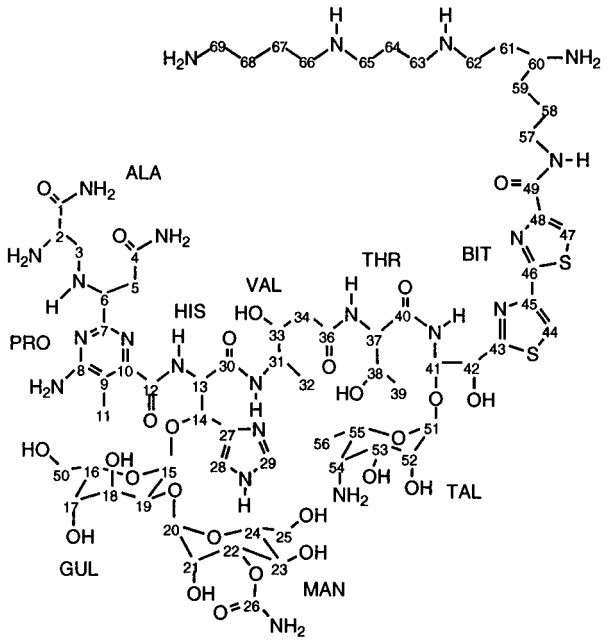

Figure 1. Tallysomycin A.

NMR and molecular modeling techniques have produced the most useful insight into the ligand arrangement in M−BLM complexes.[15−18] Recent reports of the solution structures of the hydroperoxide Co(III)$BLMA_2$ ($CoBLMA_2$ green; A_2 refers to a derivative with a specific cationic C terminus) and aqua-Co(III)$BLMA_2$ ($CoBLMA_2$ brown) forms were based on 2D NMR spectroscopy data and molecular dynamics calculations.[17,18] For both forms, the five nitrogen donors of $BLMA_2$ adopt an sp arrangement: The axial donor is the β-aminoalanine (ALA) primary amine (NC2); the equatorial donors are the ALA secondary amine (NC3), the pyrimidinylpropionamide (PRO) pyrimidine nitrogen (NC10), the β-hydroxyhistidine (HIS) deprotonated amide nitrogen (NC12), and the HIS imidazole nitrogen (NC29).

Although it was one of the first metal species to be studied, the results for $ZnBLMA_2$ are still not clear, and the differences compared to findings with other metals have led to a call for further study.[19] Several models have been proposed for $ZnBLMA_2$. Initially, both tetrahedral and octahedral models were proposed for ZnBLM.[20−22] Recently, from ^{13}C and ^{113}Cd NMR results on $CdBLMA_2$, it was suggested that at most four N donors were bound to Cd and, by analogy, to Zn.[23] A recent octahedral model for $ZnBLMA_2$ (five typical N donors and the mannose carbamoyl moiety) was suggested by combined 2D NMR and distance geometry methods and the ^1H and ^{13}C NMR shifts upon complexation.[15,24]

Despite the obvious importance of chirality in drug−DNA interactions, only recently have investigators focused on the chirality of the metal center. Considerable effort has been expended in determining the chirality of the carbons in the antibiotics and in the development of elegant syntheses to prepare these complicated natural products.[25−30] We report for the first time a complete NMR-based structural determination of ZnTLMA including restrained molecular mechanics and molecular dynamics (MM/MD) calculations, comparison of experimental and simulated spectra, and NMR *R*-factor calculations.

Experimental Section

Preparation of ZnTLMA and TLMA. TLMA·*n*HCl (Bristol Myers Lot 80F420) and $ZnCl_2$ (Aldrich) were used without further purification. The concentration of a stock $ZnCl_2$ solution, made by dissolving $ZnCl_2$ in deionized water, was determined by titration with a standard EDTA solution (0.1 M). The stock $ZnCl_2$ solution, after being lyophilized three times and dissolved in D_2O, was used to titrate a TLMA solution. The degree of complexation was monitored by NMR (a published pulse sequence[31] was used in H_2O). After lyophilization, the samples were dissolved in 99.8% D_2O (0.5 mL). The pH (uncorrected) was adjusted with NaOD (or DNO_3), and the solution was lyophilized. Finally, the ZnTLMA samples (25 mM) were dissolved in 99.98% D_2O (0.5 mL). The ZnTLMA sample (35 mM) for H_2O (90%)/D_2O (10%) experiments was prepared in an analogous manner.

Electrospray Mass Spectrometry (EMS). The EMS solutions, prepared as described above, were first checked by ^1H NMR. Mass spectra of TLMA, $BLMA_2$, and their Zn complexes were obtained using a Jeol JMS-SX102/SX102A/E mass spectrometer. Ion source 1 was a JEOL Generation 2 ESI source operated at 5 kV. The precursor ions were electrosprayed from a solution of 50:50 CH_3OH/H_2O in which the compounds were at a concentration of 10 mM. The mass resolution of the spectrometer was 1000 or 3000 so that the charge state of the species could be identified unambiguously. The ion source capillary and skimmers were tuned to optimize transmission and minimize the kinetic energy distribution of the precursor ions.

NMR Spectroscopy. 1D ^1H NMR spectroscopy was performed on Nicolet NB-360 MHz and GE GN-500 MHz spectrometers. 1−1 echo experiments[32] were carried out in H_2O (90%)/D_2O (10%) in order to obtain the optimal temperature and pH conditions for the ZnTLMA complex NMR studies. The exact ^{13}C shifts of the ZnTLMA and TLMA samples were measured at 22 °C from a 1D spectrum recorded on GE Ω-600 and GE QE-300 spectrometers, respectively. Both ^{13}C and ^1H chemical shifts were referenced to sodium 3-(trimethylsilyl)-tetradeuteriopropionate (TSP). 2D NMR experiments on the ZnTLMA sample were performed at 22 °C (pH 4.5, 6.7) or 1 °C (pH 4.5) on a GN-500 or Ω-600 spectrometer. 2D NMR experiments on the TLMA sample were performed at 30 °C on a GN-500 spectrometer. The 2D NMR experiments, performed without sample spinning, were processed with FELIX (Biosym/MSI). The homonuclear 2D NMR spectra were zero-filled to 2048 × 2048 real points.

Phase-Sensitive NOE Spectroscopy (NOESY).[33] NOESY spectra resulted from a 512 × 2048 (GN-500) and a 1024 × 2048 (Ω-600) data matrix size with 16 scans per t_1 value. Predelays were 1.0 s

(15) Akkerman, M. A. J.; Haasnoot, C. A. G.; Hilbers, C. W. *Eur. J. Biochem.* **1988**, *173*, 211−225.
(16) Akkerman, M. A. J.; Neijman, E. W. J. F.; Wijmenga, S. S.; Hilbers, C. W.; Bermel, W. *J. Am. Chem. Soc.* **1990**, *112*, 7462−7474.
(17) Xu, R. X.; Nettesheim, D.; Otvos, J. D.; Petering, D. H. *Biochemistry* **1994**, *33*, 907−916.
(18) Wu, W.; Vanderwall, D. E.; Lui, S. M.; Tang, X. J.; Turner, C. J.; Kozarich, J. W.; Stubbe, J. *J. Am. Chem. Soc.* **1996**, *118*, 1268−1280.
(19) Stubbe, J.; Kozarich, J. W.; Wu, W.; Vanderwall, D. E. *Acc. Chem. Res.* **1996**, *29*, 322−330.
(20) Dabrowiak, J. C.; Greenaway, F. T.; Grulich, R. *Biochemistry* **1978**, *17*, 4090−4096.
(21) Lenkinski, R. E.; Dallas, J. L. *J. Am. Chem. Soc.* **1979**, *101*, 5902−5906.
(22) Oppenheimer, N. J.; Rodriguez, L. O.; Hecht, S. M. *Biochemistry* **1979**, *18*, 3439−3445.
(23) Otvos, J. D.; Antholine, W. E.; Wehrli, S.; Petering, D. H. *Biochemistry* **1996**, *35*, 1458−1465.
(24) Akkerman, M. A. J.; Haasnoot, C. A. G.; Pandit, U. K.; Hilbers, C. W. *Magn. Reson. Chem.* **1988**, *26*, 793−802.
(25) Aoyagi, Y.; Katano, K.; Suguna, H.; Primeau, J.; Chang, L.-H.; Hecht, S. M. *J. Am. Chem. Soc.* **1982**, *104*, 5537−5538.
(26) Aoyagi, Y.; Suguna, H.; Murugesan, N.; Ehrnfeld, G. M.; Chang, L.-H.; Ohgi, T.; Shekhani, M. S.; Kirkup, M. P.; Hecht, S. M. *J. Am. Chem. Soc.* **1982**, *104*, 5237−5239.
(27) Boger, D. L.; Colletti, S. L.; Honda, T.; Menezes, R. F. *J. Am. Chem. Soc.* **1994**, *116*, 5607−5618.
(28) Boger, D. L.; Honda, T.; Dang, Q. *J. Am. Chem. Soc.* **1994**, *116*, 5619−5630.
(29) Boger, D. L.; Honda, T.; Menezes, R. F.; Colletti, S. L. *J. Am. Chem. Soc.* **1994**, *116*, 5631−5646.
(30) Boger, D. L.; Honda, T. *J. Am. Chem. Soc.* **1994**, *116*, 5647−5656.
(31) Redfield, A. G.; Kunz, S. D.; Ralph, E. K. *J. Magn. Reson.* **1975**, *19*, 114−117.
(32) Sklenar, V.; Bax, A. *J. Magn. Reson.* **1987**, *74*, 469−479.
(33) States, D. J.; Haberkorn, R. A.; Ruben, D. J. *J. Magn. Reson.* **1982**, *48*, 286−292.

(ZnTLMA) and 2.0 s (TLMA). The mixing time (t_m) was 300 ms. For the ZnTLMA complex, a 2 Hz exponential line broadening function followed by a cubic spline baseline correction routine and a 90° shifted sine bell squared filter were used prior to Fourier transformation (FT) in the t_2 and t_1 dimensions, respectively. For TLMA, a 90° shifted sine bell squared filter over the first 1024 points was used in both dimensions prior to FT.

NOESY in H_2O. The NOESY spectrum of the ZnTLMA complex in H_2O was obtained on the GN-500 at 1 °C and pH 4.5. The NOESY pulse sequence was modified by replacing the last 90° pulse with a 1−1 echo sequence [$90°_x - \tau - 90°_{-x} - \Delta_1 - 90°_\phi - (2\tau + \delta) - 90°_{-\phi} - \Delta_2$].[32,34] No decoupler pulse for water presaturation was used during data acquisition. The carrier frequency was set to 5.01 ppm and the H_2O resonance at 1 °C. To maximize the NH signals, the delays τ, δ, Δ_1, and Δ_2 were adjusted ($\tau = 65$ μs, $\delta = 10$ μs, $\Delta_1 = 142$ μs, and $\Delta_2 = 112$ μs). A 50 ms homospoil pulse with a 512/2047 Z-gradient was used during $t_m = 190$ ms. The spectrum was acquired with 4096 real points in t_2 and 256 t_1 increments. The spectral width was 8000 Hz in both dimensions, and 128 scans were acquired per t_1 value. The 90° pulse for H_2O suppression was 12.5 ms with a recycle delay of 2 s. A 0.5 Hz exponential line broadening function was used prior to FT in the t_2 dimension; zero-order polynomial and cubic spline baseline correction routines were also applied. A 90° phase shifted sine bell squared filter was used prior to FT in the t_1 dimension.

Double Quantum Filtered COSY (DQFCOSY).[35] The DQFCOSY spectrum of ZnTLMA (Ω-600) resulted from a 512 × 2048 data matrix size with 32 scans per t_1 value with presaturation of the residual HOD peak. A 4 Hz Gaussian line broadening function and a 90° phase shifted sine bell squared filter were used prior to FT in the t_1 and t_2 dimensions, respectively.

Phase Sensitive ^{1}H−^{1}H Correlation Spectroscopy (PSCOSY).[36] The PSCOSY spectrum of TLMA (GN-500) resulted from a 512 × 1024 data matrix size with 16 scans (preceded by 4 dummy scans) per t_1 value. Each acquisition contained a 2 s presaturation pulse to minimize the intensity of the HOD signal and a 500 ms predelay. Each dimension was apodized with a 0° phase shifted sine bell squared filter over the first 1024 points prior to FT.

^{1}H-Detected Heteronuclear Multiple Quantum Coherence Spectroscopy (HMQC).[37] The HMQC spectra of ZnTLMA (Ω-600) and TLMA (GN-500) resulted from a 128 × 2048 data matrix size with 400 (ZnTLMA) and 384 scans (TLMA) (preceded by 4 dummy scans) per t_1 value. The predelay was 1.0 s; 27 μs and 38 μs 90° ^{13}C pulse widths and 71 dB and 63 dB of ^{13}C rf power, for ZnTLMA and TLMA, respectively, were used. Prior to FT in both the t_1 and t_2 dimensions, 90° (ZnTLMA) and 30° (TLMA) phase shifted sine bell squared filters were used.

For TLMA, in order to resolve the many ^{13}C resonances in the 30−80 ppm range, a second HMQC spectrum with a higher digital resolution in the ^{13}C dimension was acquired. This spectrum resulted from a 272 × 2048 data matrix size with 336 scans (preceded by 4 dummy scans) per t_1 value. Spectral widths of 4761.9 and 6418.5 Hz were used in the ^{1}H and ^{13}C dimensions, respectively. The predelay was 1.2 s; 90° and 0° phase shifted sine bell squared filters were used prior to FT in the t_1 and t_2 dimensions, respectively.

^{1}H-Detected Multiple-Bond Heteronuclear Multiple Quantum Coherence Spectroscopy (HMBC).[38] The HMBC spectra of ZnTLMA and TLMA resulted from 256 × 2048 (Ω-600) and 192 × 2048 (GN-500) matrixes, respectively, with 400 (ZnTLMA) and 480 (TLMA) scans (preceded by 4 dummy scans) per t_1 increment. Predelays were 1.0 s (ZnTLMA) and 1.2 s (TLMA); 27 μs and 38 μs 90° ^{13}C pulse widths and 71 dB and 63 dB of ^{13}C rf power, for ZnTLMA and TLMA, respectively, were used. The delay between the first 90° ^{1}H pulse and the first 90° ^{13}C pulse was 3.3 ms. The delay between the first and the second 90° ^{13}C pulses was 53.3 ms. For ZnTLMA, 30° and 45° phase shifted sine bell squared filters were used prior to FT in the t_1 and t_2 dimensions, respectively. For TLMA, 45° phase shifted sine bell squared filters were used prior to FT in both dimensions.

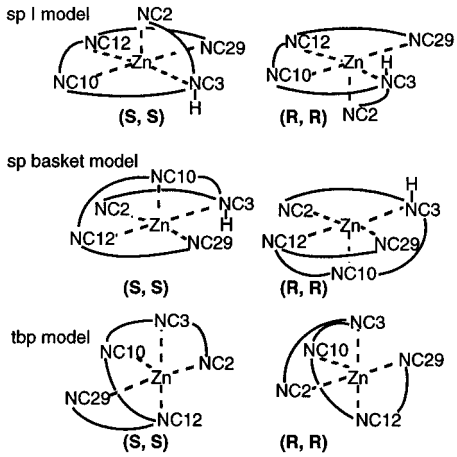

Figure 2. sp I, sp basket, and tbp models for the ZnTLMA complex, showing the two possible configurations, with indication of the Zn and NC3 chiralities (Zn, NC3).

NOESY Back-Calculations. NOESY data were collected on the Ω-600 at 1 °C and pH 4.5 at $t_m = 5$, 50, 100, 250, and 500 ms. The NOESY back-calculations were performed using the programs BK-CALC, GNOE, and FELIX (Biosym/MSI).

The complete time course for nuclear relaxation was determined via numerical integration of the Bloch equations. This approach, described elsewhere,[39] accounts for spin-diffusion peaks. The algorithm BK-CALC uses an empirical two-parameter fitting of the spectral density. These parameters are the cross relaxation rate constant (k_{cr}), which governs the cross relaxation rate, and the Z-leakage rate constant (k_{zl}), which accounts for the loss of Z-magnetization during t_m due to all processes other than cross relaxation. k_{cr} (60 s^{-1}) was determined by fitting the NOE buildup curves of well-resolved geminal methylene protons (e.g., C34H′ and C34H″) with a structurally well-defined internuclear distance of 1.8 Å. This k_{cr} value is in the range of reported values for a coenzyme F430 ($k_{cr} = 75$ s^{-1})[39] and an HIV zinc finger ($k_{cr} = 60$ s^{-1}).[40] k_{zl} (1 s^{-1}, except 3 s^{-1} for methyl protons) was determined by measuring the rate of loss of total spectral magnetization as a function of increasing t_m.[39]

The results of the NOESY back-calculations were then brought into GNOE. Consecutive serial files, obtained from the GNOE calculations for different t_m values, were incorporated into FELIX to display the NOESY back-calculated spectra, which were visually compared with the experimental spectra. Visual comparison was important because it enabled comparison of overlapped peaks that could not be included in the *R*-factor calculations (see below).

NOE-Derived Interproton Distance Restraints. The volumes of well-resolved NOESY cross-peaks were obtained by direct integration using the "box method" in FELIX 2.30. These volumes were used to generate the NOE restraints using the distances of the C34H′−C34H″ and C61H′−C61H″ proton pairs (1.8 Å) as references for the proton pairs in the molecule. Interproton distance restraints of 2.0−2.5, 2.5−3.5, and 3.5−5.5 Å were used for strong, medium, and weak NOE cross-peaks, respectively. Pseudoatoms were used for methyl protons and for geminal methylene protons with overlapping signals that could not be stereospecifically assigned. A 1.0 Å distance correction was added to the upper bound distance for the proton pairs involving methylene and methyl pseudoatoms. Spin-diffusion peaks were identified on the basis of the experimental NOE buildup profiles at different t_m values.

Molecular Mechanics/Molecular Dynamics Calculations. The structures for ZnTLMA (Figure 2) were constructed using InsightII. Bond lengths and bond angles of the covalent linkages for which no crystal structures are reported were based on average values of similar

(34) Blake, P. R.; Summers, M. F. *J. Magn. Reson.* **1990**, *86*, 622−625.
(35) Muller, N.; Ernst, R. R.; Wuthrich, K. *J. Am. Chem. Soc.* **1986**, *108*, 6482−6492.
(36) Macura, S.; Huang, Y.; Suter, D.; Ernst, R. R. *J. Magn. Reson.* **1981**, *43*, 259−281.
(37) Bax, A.; Subramanian, S. *J. Magn. Reson.* **1986**, *67*, 565−569.
(38) Bax, A.; Summers, M. F. *J. Am. Chem. Soc.* **1986**, *108*, 2093−2094.
(39) Won, H.; Olson, K. D.; Hare, D. R.; Wolfe, R. S.; Kratky, C.; Summers, M. F. *J. Am. Chem. Soc.* **1992**, *114*, 6880−6892.
(40) Summers, M. F.; South, T. L.; Kim, B.; Hare, D. H. *Biochemistry* **1990**, *29*, 329−340.

systems. MM/MD calculations were carried out using InsightII/Discover (Biosym/MSI) and the Biosym AMBER force field, modified to account for the Zn. The van der Waals force field parameters related to the Zn and Zn−N bond lengths were $R^*(\mathrm{Zn}) = 1.1$ Å, $\epsilon(\mathrm{Zn}) = 0.0125$ kcal mol^{-1},[41] $r(\mathrm{Zn-N}) = 2.00-2.20$ Å, and $K_r(\mathrm{Zn-N}) = 100$ (200 for some geometries) kcal mol^{-1} Å^{-2}.[42,43] Equilibrium N−Zn−N bond angles were taken as 90°, 180°, and 120° (depending on the geometry) with a force constant of 30 kcal mol^{-1} rad^{-2}. A 60 kcal mol^{-1} rad^{-2} force constant was used for the other Zn-related angles.[42] Since the torsional force constants for all the rotations involving Zn were set to zero, these rotation barriers did not influence the refined geometry of the complex.[41]

The MM/MD calculations were carried out in vacuo with a distance-dependent dielectric constant ($4r$). We used a restraint file including (a) a total of 73 NOE restraints, (b) 641 push-apart restraints to constrain proton pairs that show peaks in the back-calculated spectra, but not in the experimental spectra, and (c) chiral restraints for 23 of the TLMA chiral carbons. The NOE restraints for our calculations as well as NOEs previously reported for $ZnBLMA_2$,[15] $CoBLMA_2$,[17,18] and $BLMA_2$-FeCO[16] are shown in the Supporting Information. Carbon stereochemical assignments were taken from studies of the absolute configuration of $BLMA_2$ and derivatives.[27−30] No chiral restraints for C41, C42, and C60 were used. Nevertheless, on the basis of experimental NOE cross-peak intensities, the stereochemistries of C41 and C42 were found to be *S*. Because of signal overlap, the C60 absolute configuration could not be assigned.

The MM/MD protocol used consisted of the following steps: (a) restrained energy minimization by the steepest descent method for 200 cycles, (b) 0.5 ps equilibration during which the structure was heated to 2000 K, (c) 5 ps restrained dynamics at 2000 K with trajectories saved every 1 ps, and (d) minimization of the saved trajectories first by the steepest descent method for 200 cycles and then by a conjugate gradient method for 50 000 cycles or until a maximum derivative of 0.001 kcal/(mol Å) was achieved.

The lowest energy MM/MD structure with the best overall agreement between experimental and back-calculated spectra from this protocol was then refined by IRMA (iterative relaxation matrix approach).[44] We used a hybrid experimental/model relaxation matrix calculation containing an MM/MD protocol similar to the one described above except that (b) and (c) were as follows: (b) 3 ps equilibration during which the structure was heated from 20 to 300 K in steps of 20 K every 0.2 ps and (c) 25 ps restrained dynamics at 300 K with trajectories saved every 1 ps. The calculations were carried out considering four t_m values (i.e., 50, 100, 250, and 500 ms).

The quality of the MM/MD-IRMA structures was evaluated on the basis of three criteria: the total potential energy, the consistency between experimental and back-calculated NOESY spectra, and the NOE-based *R*-factors of the structures.[45] We used $R_r = (\sum(|A_{calc}|^{-1/6} - |A_{exp}|^{-1/6})^2/\sum(|A_{exp}|^{-1/3}))^{1/2}$ and $R_1 = \sum(|A_{calc} - A_{exp}|)/\sum(|A_{exp}|)$, where A_{calc} and A_{exp} denote theoretical and experimental NOE intensity matrix elements, respectively.

The following methodologies were used to analyze the MM/MD-IRMA structures (analysis protocol). First, the *R*-factors and simulated spectra at different t_m values (i.e., 100, 250, and 500 ms) were determined for the lowest energy structure (final IRMA structure) from two runs (50 structures each) using a different initial MM/MD structure. If these two were very similar, we concluded there was no starting structure dependence. Second, the final IRMA structure was evaluated by further minimization without using the NOE restraints. If the structure did not change significantly, we assumed we were near the energy minimum. Third, the coordinates of the 10 lowest energy IRMA structures from one run were averaged and minimized to give an average structure. Each of the 10 structures was compared to the average structure to ascertain that these formed a family of closely related structures.

Results

Assignment of the ^{1}H and ^{13}C NMR Spectra. Addition of $ZnCl_2$ to TLMA led to the observation of new signals for the 1:1 complex, indicating slow exchange on the NMR time scale. After the ZnTLMA complex was fully formed, addition of an excess of Zn (up to 2 equiv) did not affect the ^{1}H and ^{13}C NMR spectra. Thus, unlike Ni(II) and Cu(II),[46] Zn(II) does not form a M_2−TLMA complex. Assignments of the ^{1}H and ^{13}C NMR signals of both TLMA and ZnTLMA (Supporting Information) by 2D NMR strategies used previously[47] are described in the Supporting Information. Our ^{13}C assignments differ from those reported previously[48] (Supporting Information). The ^{13}C nuclei are designated numerically in Figure 1. The ^{1}H nuclei are designated by the carbon atom to which they are attached. For nonequivalent geminal resonances, H′ and H″ refer to the downfield and upfield signals, respectively. Some of the ^{1}H chemical shifts depended on the temperature, whereas no noticeable differences in chemical shifts were detected between pH 4.5 and pH 6.7 (Supporting Information). Our studies suggest that the NOESY experiments of the ZnTLMA complex at 1 °C and pH 4.5 are more informative than those at 22 °C and pH 6.7. For this reason, the discussion will be focused on the 1 °C spectra, except for the heteronuclear NMR experiments at 22 °C (Supporting Information).

Comparison to $ZnBLMA_2$. The ^{13}C and ^{1}H NMR assignments of the ZnTLMA (pH 4.5) complex in D_2O are virtually identical to those of $ZnBLMA_2$ (pH 6.7), excluding the tail and the talose (TAL) region (Supporting Information). In addition, the ^{13}C and ^{1}H chemical shift changes upon Zn binding, ^{13}C $\Delta\delta$ and ^{1}H $\Delta\delta$ ($\Delta\delta = \delta_{ZnL} - \delta_L$), were very similar. Thus, although the pH values were different, these similarities in $\Delta\delta$ demonstrate that the core coordination environments are the same for ZnTLMA and $ZnBLMA_2$.

Tentative binding sites in $ZnBLMA_2$ were deduced on the basis of the $\Delta\delta$ values.[15,22,24] We assessed the ZnTLMA system in the same way. The upfield ^{13}C $\Delta\delta$ values of C3 (−3.0 ppm) and C6 (−3.9 ppm) and downfield ^{13}C $\Delta\delta$ of C1 (1.4 ppm) in ZnTLMA support a ligand binding model similar to that proposed for $ZnBLMA_2$,[24] with both amine nitrogens of the ALA fragment binding to Zn. Likewise, the large downfield ^{13}C $\Delta\delta$ values for C8 (3.2 ppm) and C9 (1.9 ppm) and upfield ^{13}C $\Delta\delta$ values for C7 (−4.1 ppm) and C10 (−3.5 ppm) in ZnTLMA suggest participation of the pyrimidine ring in Zn binding, probably through NC10.

Only small ^{13}C $\Delta\delta$ values of ∼0.6 ppm for the imidazole carbons were observed for ZnTLMA (pH 4.5) and $ZnBLMA_2$ (pH 6.7).[24] In the pH range 4−6.7, the $BLMA_2$ C27 and C29 resonances show an appreciable ^{13}C $\Delta\delta$ (−5.5 and −2.4 ppm, respectively) because the imidazole pK_a is 5.3.[49] Likewise, for tallysomycin s_{10b}, which differs from TLMA only in the tail region, C27 and C29 shifted −5.2 and −2.1 ppm, respectively.[47] Similar ^{13}C $\Delta\delta$ values are expected for the TLMA imidazole signals in this pH range. The absence of significant C27 and C29 ^{13}C $\Delta\delta$ values for ZnTLMA (pH 4.5) vs TLMA (pH 6.7)

(41) Chapotchartier, M. P.; Rul, F.; Nardi, M.; Gripon, J. C. *Eur. J. Biochem.* **1994**, *224*, 497−506.
(42) Adam, K. R.; McCool, B. J.; Leong, A. J.; Lindoy, L. F.; Ansell, C. W. G.; Baillie, P. J.; Dancey, K. P.; Drummond, L. A.; Henrick, K.; McPartlin, M.; Uppal, D. K.; Tasker, P. A. *J. Chem. Soc., Dalton Trans.* **1990**, 3435−3444.
(43) Orpen, A. G.; Brammer, L.; Allen, F. H.; Kennard, O.; Watson, D. G.; Taylor, R. *J. Chem. Soc., Dalton Trans.* **1989**, S1-S83.
(44) Boelens, R.; Koning, T. M. G.; van der Marel, G. A.; van Boom, J. H.; Kaptein, R. *J. Magn. Reson.* **1989**, *82*, 290−308.
(45) Gonzalez, C.; Rullmann, J. A. C.; Bonvin, A. M. J. J.; Boelens, R.; Kaptein, R. *J. Magn. Reson.* **1991**, *91*, 659−664.
(46) Greenaway, F. T.; Dabrowiak, J. C.; Van Husen, M.; Grulich, R.; Crooke, S. T. *Biochem. Biophys. Res. Commun.* **1978**, *85*, 1407−1414.
(47) Freyder, C. P.; Marzilli, L. G. *Magn. Reson. Chem.* **1991**, *29*, 338−350.
(48) Greenaway, F. T.; Dabrowiak, J. C.; Grulich, R.; Crooke, S. T. *Org. Magn. Reson.* **1980**, *13*, 270−273.
(49) Mooberry, E. S.; Dallas, J. L.; Sakai, T. T.; Glickson, J. D. *Int. J. Pept. Res.* **1980**, *15*, 365−376.

demonstrates that the imidazole is bound; otherwise, it would be protonated, and large ^{13}C $\Delta\delta$ values would have been observed.

Likewise, ^{1}H $\Delta\delta$ values were used to assess which moieties were bound to Zn. Participation of the primary amine (NC2) and secondary amine (NC3) of ALA in Zn binding is supported by significant ^{1}H $\Delta\delta$ values (~0.2−0.6 ppm) of the C2H, C3H″, C3H′, C5H″, C5H′, and C6H signals; these are similar to ^{1}H $\Delta\delta$ values for $ZnBLMA_2$.[15] Furthermore, the presence of the H′NC2, H″NC2, and HNC3 ^{1}H signals in the NOESY spectrum in H_2O (Supporting Information) demonstrates that NC2 and NC3 are Zn binding sites in ZnTLMA since protons of unbound amines exchange too rapidly for ^{1}H signals to be observed.[15] Similarly, the resonances of the NC2 and NC3 protons of $BLMA_2$ were detected only upon complexation to Zn.[15] The downfield ^{1}H $\Delta\delta$ of C29H (0.26 ppm) is consistent with imidazole binding. The binding of the TLMA pyrimidine ring suggested by ^{13}C $\Delta\delta$ is supported by a significant downfield ^{1}H $\Delta\delta$ (0.38 ppm) of Me11.

For ZnTLMA, most of the VAL ^{1}H $\Delta\delta$ values are upfield (ca. −0.25 ppm). The similar $\Delta\delta$ values for $ZnBLMA_2$ were attributed to the proximity of the VAL protons to the π-electrons of the imidazole in the proposed $ZnBLMA_2$ model.[15] If VAL were coordinated, the ^{13}C signals would be expected to shift significantly, but they do not. In our ZnTLMA models, the VAL is involved in H-bonding through the VAL hydroxyl or amide groups, perhaps accounting for these $\Delta\delta$ values. The small ^{1}H $\Delta\delta$ values (in general, <0.1 ppm) for ZnTLMA for THR, BIT, and the tail moieties suggest that these residues are not involved in metal binding.

Downfield ^{13}C $\Delta\delta$ values for C12 and C13 (1.3 and 4.0 ppm, respectively) and the absence of the HNC12 ^{1}H signal suggest that the HIS deprotonated amide group is bound to Zn even at pH 4.5. The binding to Zn of the deprotonated amide nitrogen of a BLM analog (Figure 3) was demonstrated by X-ray crystallography.[14]

In summary, the ^{1}H and ^{13}C $\Delta\delta$ data are consistent with the following Zn binding sites to TLMA: the ALA amines NC2 and NC3, the pyrimidine NC10, and the deprotonated amide nitrogen (NC12) and an imidazole nitrogen (NC29 or NC28) of the HIS residue.

Electrospray Mass Spectrometry. TLMA and $BLMA_2$ have monoisotopic molecular weights of 1731.9 and 1414.5, respectively. The EMS spectrum of ZnTLMA in $MeOH/H_2O$ showed a peak at a mass to charge ratio (m/z) of 898.1. This peak was assigned to the singly protonated, doubly charged ZnTLMA, $[ZnTLMA^{+} + H^{+}]^{2+}$ (m/z = 898.1). Likewise, the peak with m/z = 739.5 in the EMS spectrum of $ZnBLMA_2$ in $MeOH/H_2O$ was assigned to the singly protonated, doubly charged $ZnBLMA_2$ (m/z = 739.9). Although EMS data do not provide information about the three-dimensional structure of these species, these m/z values are most consistent with monomeric ZnTLMA and $ZnBLMA_2$ complexes.

Molecular Mechanics/Molecular Dynamics Calculations. Metal complexation to TLMA or BLM stabilizes two chiral centers, at the metal atom and the secondary amine, NC3. These chiral centers must be defined. We employed the Cahn−Ingold−Prelog (*R* and *S*) system[50,51] to indicate the absolute configuration of the chiral atoms. To define the chirality of the metal in the five-coordinate models, we selected four N atoms ranked in decreasing order of priority as follows: NC10, NC29 (or NC28), NC3, and NC2. For example, *SS* or *RR* denotes [Zn(*S*), NC3(*S*)] and [Zn(*R*), NC3(*R*)], respectively. For models in which NC2 is not bound and the other four N atoms are in the equatorial plane, we designate metal chirality by assuming that NC2 binds to the nearest axial site.

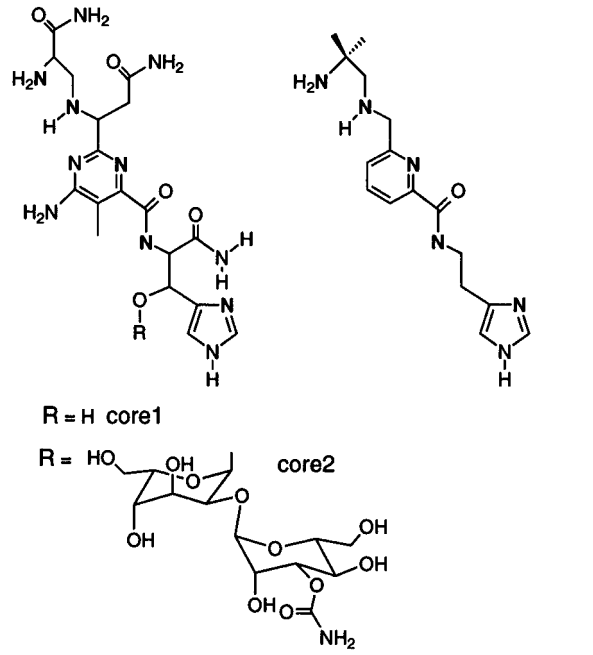

Figure 3. Left: Binding domain (core 1) and extended binding domain (core 2, including the dissacharide moiety). Right: A ligand analog.

We evaluated three sp ZnTLMA models, I, II, and basket (Figure 2 and the Supporting Information). The arrangement in model sp I (NC2 axial; NC3, deprotonated NC12, NC10, and NC29 equatorial) is found in some X-ray structures of M−BLM analogs.[11−13] In model sp II (Supporting Information), NC29 is in an axial position, NC2 occupies an equatorial position, and the other sites are those in model I. We have found only one report of this sp II geometry, in an MM study of Fe(III)BLM analogs.[52] In the novel sp basket model, NC10 is in an axial position, and NC2, NC3, NC12, and NC29 occupy the equatorial sites. Because of the chiralities of Zn and NC3, four configurations are hypothetically possible for each model. However, for the sp I and basket models only two of the four configurations are feasible since the position of the primary amine dictates the chirality of NC3 (Figure 2).

For the sp models, the lowest energy structures from the MM/MD calculations were selected for evaluation. Highly distorted imidazole rings and/or very distorted C6 geometries were observed for the *SS*-sp I and all sp II models. Although the *RR*-sp I and *RR*-basket models had no distortions and gave good agreement between experimental and back-calculated spectra, the chirality at some carbons had inverted. Inversion of the chirality at C6 for the *RR*-sp I and *RR*-basket models was caused by the C6H−C22H NOE restraint (see below). In contrast, for the *SS*-sp basket model neither distorted geometries nor changed chiralities were observed.

We conducted the analysis protocol outlined in the Experimental Section for the *SS*-sp basket model. The 10 lowest energy IRMA structures (Supporting Information) exhibit good superimposition of core 1 (Figures 3 and 4). The final IRMA structure has an H-bond network involving several TLMA functional groups and good *R*-factors (this and related information for other models is in the Supporting Information). The back-calculated NOESY spectra compare well with the experi-

(50) Cahn, R. S.; Ingold, C.; Prelog, V. *Angew. Chem., Int. Ed. Engl.* **1966**, *5*, 385−415.

(51) Fessenden, R. J.; Fessenden, J. S. *Organic Chemistry*, 3rd ed.; Brooks/Cole: Belmont, CA, 1986; pp 118−120, 144−149.

(52) Wu, Y.-D.; Houk, K. N.; Valentine, J. S.; Nam, W. *Inorg. Chem.* **1992**, *31*, 718−720.

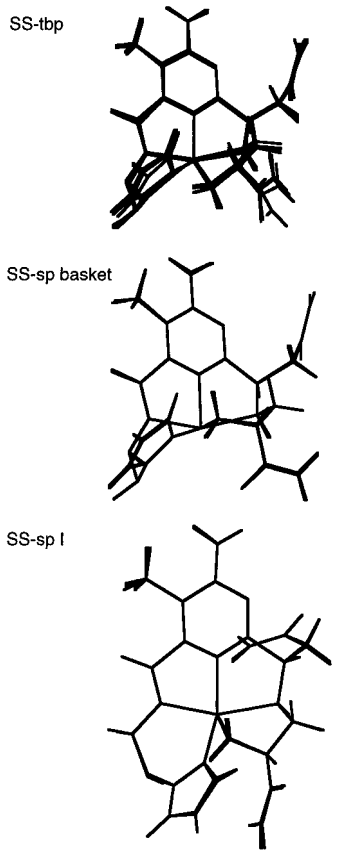

Figure 4. Superimposition of the 10 IRMA structures with the lowest potential energy for the *SS*-tbp, *SS*-sp basket, and *SS*-sp I monomer models. Only the core 1 atoms are shown.

mental spectra (Figure 5). Simulated spectra at 100 and 250 ms contained all the experimental NOEs at 100 and 250 ms, respectively; each contained several cross-peaks present in spectra at longer mixing times. The back-calculated spectrum at 500 ms contained all the strong and medium intensity NOEs present in the 500 ms experimental spectrum and all of the weak NOE cross-peaks, except C28H−(C22H, C19H).

Since the arrangements of the $BLMA_2$ metal binding domain in several models each resembled either our *SS*-sp I or our *RR*-sp I model,[15−18] we conducted an unrestrained minimization of both models. Because the total potential energy for the *SS*-sp I model was ∼90 kcal/mol lower than for the *RR*-sp I model (Supporting Information), we performed restrained MM/MD calculations on the *SS*-sp I model but with no C6H−C22H NOE restraint. The 10 selected IRMA structures are shown in Figure 4 and the Supporting Information. For the final IRMA structure, there are several hydrogen bonds in the vicinity of the Zn binding domain. The back-calculated spectrum at 500 ms contained all strong and medium and most of the weak 500 ms experimental NOEs (Figure 5). However, as expected, *no* C6H−C22H NOE cross-peak was produced in any back-calculated spectra; the weak NOE between C2H and C5H″ was also absent. In addition, some extra weak cross-peaks, mostly involving protons far from the Zn binding domain (e.g., in the tail, BIT, TAL, and VAL), were produced at all t_m values by the *SS*-sp I model, despite the push-apart distance restraints. This is an interesting result since the *SS*-sp I $CoBLMA_2$ species has experimental NOE cross-peaks to the tail.[18]

The X-ray structure of the small tbp ZnBLM analog complex[14] prompted us to evaluate a tbp ZnTLMA model (Figure 2) (NC3 and NC12 axial; NC2, NC10, and NC29 equatorial). Only two of the four configurations, namely, *SS*-tbp and *RR*-tbp, are feasible (Figure 2). During MM/MD calculations on the *RR*-tbp model, the chiralities of some carbons (e.g., C6, C15, and C22) inverted; no chirality changes were observed for the *SS*-tbp model (cf. Figure 4 and the Supporting Information). The simulated spectrum at 500 ms of the *SS*-tbp model was very similar, except for two extra, very weak cross-peaks (C63H′−C61H″, C63H″−C61H′), to the simulated spectrum of the *SS*-sp basket model (Supporting Information).

Comparing our *SS*-tbp model with the crystallographic structure of the small ZnBLM analog, we found good superimposition of the zincs, secondary amines, pyrimidine/pyridine, and amides (Figure 6; the pairwise root mean squared deviation (RMSD) value is 0.29 Å for superimposing these 15 heavy atoms per molecule). Most of the Zn−N bond distances and N−Zn−N bond angles are similar (Supporting Information). The imidazole ring and the linker carbons did not superimpose well, as discussed below.

We briefly describe an assessment of two ZnTLMA dimer models studied to see if these could fit the NOESY spectra, particularly the C6H−C22H cross-peak, better than monomers. The first dimer tested, derived from our *SS*-sp I model, gave poor results. We then tested a second dimer, with pseudo-C_2 symmetry, derived from our *SS*-sp basket model using NC2, NC3, NC10, and NC12 (from one TLMA) and the imidazole NC28 (from the other TLMA) bound to each Zn. The C6H−C29H and C22H−C6H NOEs were considered to be from two different TLMA molecules (inter-TLMA NOE). The *R*-factors for the final IRMA dimer and figures showing the superimposition of the 10 lowest energy structures appear in the Supporting Information. (The H-bonding network involving the carbamoyl and groups close to the Zn in the final dimer and other results are given in the Supporting Information.) The back-calculated and experimental NOESY spectra compared well. The simulated 500 ms spectrum (Supporting Information) contained all the NOEs present in the experimental spectrum, with only three weak extra cross-peaks, namely, C29H−C14H, C29H−C16H, and C5H″−C22H. Since fits of the experimental NMR data were reasonable, we obtained EMS data. However, the molecular weight derived from the EMS data was most consistent with a monomeric species.

A recent ^{13}C and ^{113}Cd NMR study of $CdBLMA_2$[23] suggested that, at low temperature, at most four nitrogen donors, from the pyrimidine, imidazole, and ALA primary amine and possibly from the ALA secondary amine, are bound to Cd. Therefore, we also assessed two four-coordinate ZnTLMA models. In the first model, NC2, NC3, NC10, and NC29 were the donors, and NC12 was protonated. After MM/MD, the *RR*, *RS*, and *SR* models had inverted chiralities at some carbons, including C22 and C6. In contrast, the MM/MD calculations for the *SS* model afforded a distorted tetrahedral structure without chirality changes. In this model, the amide bond of the HIS (C12−NC12) is perpendicular to the plane of the PRO pyrimidine ring. For this model, agreement between experimental and back-calculated spectra was poor. The simulated spectrum at 500 ms had several extra peaks, some of them involving NOEs between C22H and C3H′, C3H″, C5H′, Me11, and C29H. The second model, with protonated NC2 and NC12, had NC3, NC10, NC29, and OC30 as the Zn binding sites. MM/MD calculations led to inversion of C chiralities (C22 for the *SS* and *SR* models and C6 for the *RR* and *RS* models).

Two NMR *R*-factors, which are a measure of the agreement between the intensities of experimental and simulated NOESY cross-peaks of ZnTLMA, were calculated during the analysis protocol of the promising sp and tbp IRMA models. These *R*-factors, namely, R_1 and R_r (Supporting Information), were comparable to those of crambin, a small protein studied

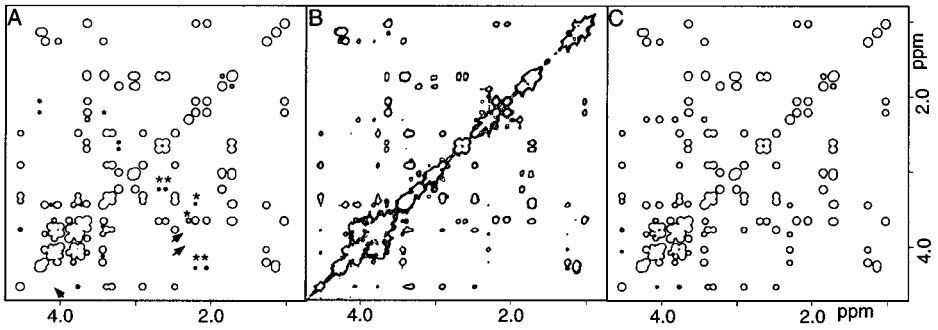

Figure 5. Back-calculated (A and C) and experimental (B) NOESY spectra of the ZnTLMA complex (500 ms) for the *SS*-sp I (A) and *SS*-sp basket (C) monomer models. In the simulated spectrum for the *SS*-sp I model, the missing cross-peaks are indicated by an arrow and the extra cross-peaks by an asterisk. A fully labeled experimental spectrum is presented in the Supporting Information.

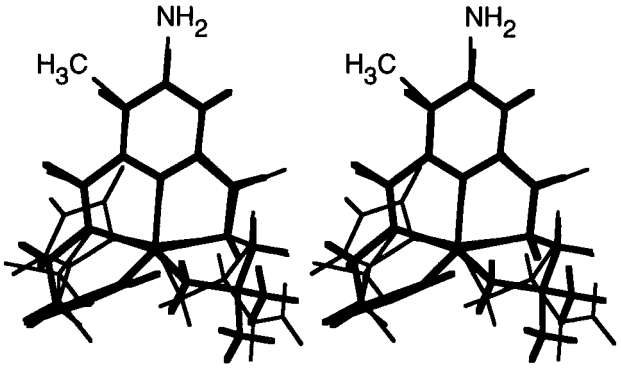

Figure 6. Comparison of (thick line) the X-ray crystallographically determined structure of the tbp Zn complex of the analog shown in Figure 3 and (thin line) the NMR-based structure of the ZnTLMA *SS*-tbp model (heavy atoms superimposed are mentioned in the text). In the stereoview, some ZnTLMA atoms are labeled to orient the reader.

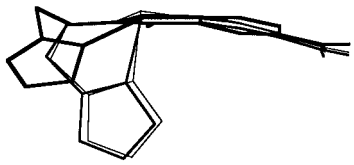

Figure 7. A view of the plane of the superimposed heavy atoms of the five-membered chelate ring (NC10, C10, C12, NC12, and Zn) and the adjacent atoms (C7, C9, OC12, and C13) of three ZnTLMA models, *SS*-sp I (thick line), *SS*-sp basket (thin line), and *SS*-tbp (medium line). For these 27 (9 + 9 + 9) atoms, the RMSD is 0.12 Å. The five-membered imidazole ring is also shown to emphasize the very different location of this group in the *SS*-sp I model.

extensively by NMR.[45] The R_1 values for NOEs involving the core 1 protons (Figure 3) were lower than the R_1 values for NOEs involving the core 2 protons (Figure 3). In addition, for all models, the core 1 R_1 values are significantly lower than the R_1 values for all other NOEs. A similar trend but with smaller differences was also observed for R_r. These data suggest that the core 1 is better defined than the rest of the molecule, as expected from the RMSD values (Supporting Information). In addition, the absence of long-range NOEs between protons in the core 2 residues to protons in the VAL, THR, TAL, BIT, and tail residues resulted in more diverse conformations for these residues, especially for the BIT and tail regions.

The R_r values were slightly lower in the *SS*-sp basket and *SS*-tbp models (∼0.20) than in the *SS*-sp I model (0.25; for the calculations of *R*-factors of the *SS*-sp I model, the C6H−C22H NOE was not included). Likewise, the R_1 values for the *SS*-sp basket and *SS*-tbp models (∼0.46) were lower than for the *SS*-sp I model (0.61). Since R_1 values are strongly influenced by short-range contacts,[45] this may indicate that the strong NOEs, which correspond to the cross-peaks with the least error, are better simulated for the *SS*-sp basket and *SS*-tbp models. Furthermore, the core 1 and core 2 R_1 values for the *SS*-sp basket and *SS*-tbp models were significantly lower than those for the *SS*-sp I model, indicating that the former models reflect the Zn binding domain of ZnTLMA better than the latter.

Minimization starting from these *SS*-sp basket, *SS*-sp I, and *SS*-tbp final IRMA models but without using NOE distance restraints yielded similar structures, especially for the Zn binding domain. Although the total potential energies of the final IRMA models depend on geometry, the total potential energy (∼220 kcal/mol) for the three resulting unrestrained *SS* monomer models was independent of geometry. Furthermore, the three unrestrained *SS* monomer models had total potential energies lower than for the corresponding unrestrained *RR* models (by ∼130, 90, and 45 kcal/mol for the basket, sp I, and tbp models, respectively).

Discussion

TLMA clearly has the same ligation sites as BLM. In this first characterization by restrained MM/MD calculations of a metal TLMA complex, we assessed many starting ZnTLMA models, including those based on all reasonable previously proposed M−BLM models. We shall discuss only the four best ZnTLMA models (the *SS*-sp basket monomer, *SS*-tbp monomer, *SS*-sp monomer, and *SS*-sp basket dimer); these have significant differences in the Zn environment, but comparable Zn−N distances (Supporting Information). Four of the donors in the four ZnTLMA models are the ALA secondary amine (NC3), the PRO pyrimidine (NC10), and the HIS amide (NC12) and imidazole (NC29). 2D NMR and molecular modeling studies of several M−BLMs[15−18] favor these same four donors, amid controversy regarding the other $BLMA_2$ donors (cf. the Introduction). To our knowledge, no analysis of the chirality of NC3 in M−BLMs has been reported, and only three studies[17,18,52] consider the chirality of the complex (two for M−BLMs[17,18] and one for a M−BLM analog[52]).

Since all four models account for almost all observations, particularly NOEs that involve exchangeable protons (Supporting Information), we describe first the common features and then features which lead us to favor some models over others. All four gave the NOEs between C29H and both C6H and HNC3; these NOEs suggest that the HIS imidazole and the ALA and the PRO residues are close to each other, as found also in $CoBLMA_2$.[17] Similarly, the ALA secondary amine and the HIS imidazole were directed toward each other in $ZnBLMA_2$[15] and $COFeBLMA_2$.[16] Thus, the coordination of this part of the metal binding domain of such antibiotics does not appear to depend on the nature of the metal.

Since no long-range NOEs between protons in the metal binding domain and protons in the BIT and tail residues were

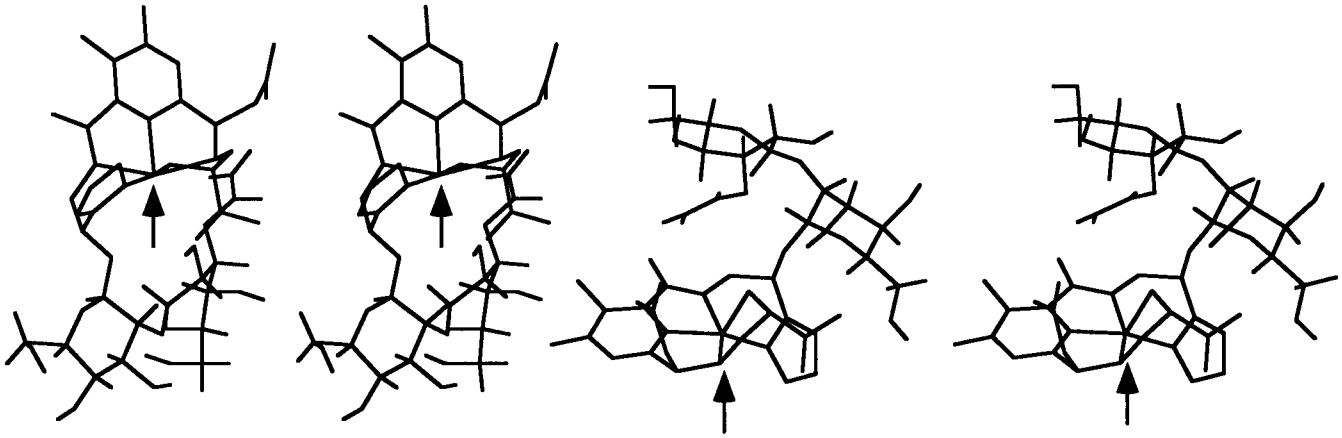

Figure 8. Stereoviews of core 2 of the *SS*-sp basket (left) and *SS*-sp I (right) models. For clarity, the only protons shown are those of the disaccharide moiety. The direction of approach to the sixth coordination site is indicated by an arrow.

detected for ZnTLMA, the BIT and tail moieties have extended conformations and show large flexibility in all our ZnTLMA models. Likewise, the absence of such long-range NOEs led to reports of flexibility of the BIT and tail moieties for $ZnBLMA_2$,[15] $COFeBLMA_2$,[16] and a form of $CoBLMA_2$.[17] In contrast, several long-range NOEs for $CoBLMA_2$ green[18] suggested a compact model with the BIT and tail folded back underneath the equatorial coordination plane of Co. Furthermore, the very large ^{1}H and ^{13}C $\Delta\delta$ values for Me35 and C34H in $CoBLMA_2$ green were explained by a well-defined conformation of the VAL and THR residues with the VAL directly underneath the imidazole.[17,18] The much smaller ^{1}H and ^{13}C $\Delta\delta$ values for the VAL residue in ZnTLMA, $ZnBLMA_2$, and $COFeBLMA_2$ are consistent with different conformations compared to that for $CoBLMA_2$ green.

The very large upfield ^{13}C $\Delta\delta$ values of C5 (ca. -6 ppm) are an interesting feature common to ZnTLMA and all M−BLMs.[16−18,23,24] Such a large ^{13}C $\Delta\delta$ is difficult to explain since C5 is not directly bound to a coordinated N in any proposed model. Part of our motivation in evaluating dimer models was to determine if such a model could explain the large shift. However, here too, no evident reason for the shift was found. Since the ^{13}C $\Delta\delta$ values for other signals depend on the identity of the metal, we believe that an inductive effect of the metal cannot explain the C5 ^{13}C $\Delta\delta$. If the free drug conformation causes an unusual C5 shift, changes in conformation, even if metal dependent, may lead to the similar anomalous C5 $\Delta\delta$. NMR studies on free $BLMA_2$ have suggested that conformational changes on protonation may influence shifts.[49]

We believe that the observed disaccharide ^{1}H and ^{13}C $\Delta\delta$ values for ZnTLMA reflect the change in conformation and positioning on complexation (Supporting Information). For example, in the *SS*-sp basket and *SS*-tbp monomer models, H-bonds (HNC3 to OC26, OC4 to HNC26, and OC1 to HOC21) stabilize the position of the mannose near the Zn. Comparable ^{1}H and ^{13}C $\Delta\delta$ values have also been reported for all M−BLMs.[15−18,23,24] For $ZnBLMA_2$[15,24] and $COFeBLMA_2$,[16] these $\Delta\delta$ values have been attributed to coordination of the carbamoyl group. The evidence included a large (-0.5 to -0.6 ppm) upfield ^{1}H $\Delta\delta$ for C22H. However, our study and a recent 2D NMR and MD study of $CoBLMA_2$ green[18] establish that the carbamoyl group is not a donor, although the complexes have the large upfield ^{1}H $\Delta\delta$ for C22H. In addition, no ^{113}Cd spin coupling to the carbamoyl C26 was observed for $CdBLMA_2$.[23]

Although the *SS*-sp I model is one of four ZnTLMA models that explain most of the experimental data, three considerations have prompted us to rule out the *SS*-sp I model for Zn. First, the potential and the NOE-associated energy terms are relatively high (Supporting Information). Second, R_r and especially R_1 values are higher for the *SS*-sp I model than for the *SS*-sp basket and *SS*-tbp models. Third, the *SS*-sp I model is the only one of the four best models that cannot account for the C6H−C22H NOE (Figure 5 and Supporting Information). For ZnTLMA, this NOE is present even at 100 ms; this cross-peak can also be observed in the published NOESY spectrum of $ZnBLMA_2$, although the authors made no mention of it.[15]

Compared to the other models, the *SS*-sp basket dimer has the highest potential energy and energy term associated with the NOE contribution (Supporting Information). In addition, although dissociation of a dimer species during the EMS experiment is a possibility, the EMS data favor a monomer. Finally, we could not find any features stabilizing a dimer, such as inter-TLMA hydrogen bonding. On the basis of these data, we exclude this model.

The similarity in the back-calculated spectra and NMR *R*-factor values for the *SS*-sp basket and *SS*-tbp monomer models suggests that these models are both good structural models for ZnTLMA. The values for the energy term associated with the NOE contribution were also comparable, whereas the potential energy for the *SS*-sp basket model was ∼20 kcal/mol lower than for the *SS*-tbp model (Supporting Information). Therefore, we conclude that the *SS*-sp basket model best represents the structure of ZnTLMA. Because the NMR data demonstrate that ZnTLMA and $ZnBLMA_2$[15] must have the same overall structure, we propose that $ZnBLMA_2$ also has this novel *SS*-sp basket geometry. However, we cannot rule out a structure intermediate between the basket and tbp structures or a fluxional mixture of the two conformers.

First, we consider why this ligand arrangement was overlooked. Normally, chelate rings on either side of a coordinated deprotonated amide form a meridional edge rather than a trigonal face of a coordination compound. The meridional edge is part of models such as the *SS*- or *RR*-sp I type. We were thus skeptical when the NMR results led to the *SS*-sp basket arrangement. However, the coordinated amide can maintain a high degree of planarity in the three most reasonable arrangements (Figure 7). Thus, these are *all* relatively unstrained structures. The only clear difference in the vicinity of the coordinated amide was the C14−C13−NC12−Zn torsion angle, which differs by ∼60° between the *SS*-sp I and the other two arrangements. In the *SS*-sp I arrangement, this difference leads to a position of the imidazole ring that allows it to accommodate a meridional edge. Such an edge is more consistent with a regular octahedral or square pyramidal geometry (see the next point).

Second, we consider why X-ray structures of simple models do not reveal this structure. An important difference between Zn and most other metals is the tendency of Zn to adopt readily distorted geometries, whereas crystal field effects force the other metals typically incorporated into synthetic models to adopt more regular geometries. Furthermore, much of the synthetic modeling has been based on analogs lacking the two very large substituents on the two-carbon chain linking the amide to the imidazole ring (i.e., disaccharide at C14 and the peptide chain, etc., at C13). Only in the case of one Zn analog is the geometry tbp (Figure 6).[14] However, even this geometry differs from our tbp model. The $N_{(imidazole)}-Zn-N_{(primary\ amine)}$ bond angle in our *SS*-tbp model (137°) is larger than in the small analog (123°); we attribute this difference to the presence of substituents at both linker carbons in ZnTLMA. Thus, although the X-ray structures of the small ligand BLM analogs are correct, they may not necessarily model the Zn binding domain of the glycopeptide antibiotics.

In MM/MD calculations on a six-coordinate ZnTLMA structure with an *SS*-sp basket arrangement and with H_2O or O_2 as the sixth axial ligand, we found that the energy term associated with the NOE contribution was comparable to that for the five-coordinate model. Furthermore, the simulated spectra for five- and six-coordinate *SS*-sp basket models were almost identical and compared well with the experimental NOESY spectra. These data suggested the feasibility of an *SS*-sp basket six-coordinate model. Moreover, pathways are readily envisioned for an *SS*-sp basket (or *SS*-tbp) Fe(II)BLM to add O_2 to form a six-coordinate *SS*-sp I HO_2Fe(III)BLM (analogous to the $CoBLMA_2$ green model[17,18]). If Fe(II)BLM has an *RR* arrangement, as proposed for $ZnBLMA_2$[15] and $COFeBLMA_2$,[16] *SS*-sp I HO_2Fe(III)BLM cannot be formed, other than in the unlikely inversion of the chirality both at the metal and at NC3.

The disaccharide would impede the loss or approach of a sixth ligand, e.g., O_2, in our *SS*-sp basket (Figure 8) and *SS*-tbp models. There are some experiments that bear on this point. A lower affinity for CO binding and a much slower rate of CO rebinding have been reported[53] for $FeBLMA_2$ compared to an FeBLM analog lacking the sugars. The disaccharide has a very different position in the *SS*-sp I model (Figure 8); this model has features which resemble those in some previous models.

(53) Sugiura, Y.; Kuwahara, J.; Suzuki, T. *FEBS Lett.* **1985**, *182*, 39−42.

In summary, ZnTLMA and $ZnBLMA_2$ have essentially identical binding domains. An extensive assessment of models with both new and standard features has shown that satisfactory results can be obtained only if the Zn and NC3 geometries are both *S*. Among known model types, one with an *SS* chirality and widely proposed features gave good results. However, models containing a new "basket" ligand arrangement and disaccharide positioning gave better results for Zn in sp, tbp, or octahedral geometry. The *SS*-sp basket model gave the best results, but the other conformers or a mixture of conformers cannot be ruled out.

Acknowledgment. We thank the NIH for support through Grant GM 29222. Purchase of instrumentation used in this study was funded in part by grants from the NIH and the NSF. We thank Mr. Ernest Schubert for assigning the TLMA spectra, Dr. Shijie Yao for help with initial calculations, and Professors Jenny Glusker (Fox Chase), Karl Hagen (Emory), Sidney Hecht (Virginia), Pradip Mascharak (Santa Cruz), and Dale Boger (Scripps) for useful discussions and for disclosing unpublished information. L.G.M. is a member of the Winship Cancer Center.

Supporting Information Available: Description of the ^1H and ^{13}C NMR spectral assignment for ZnTLMA; tables of ^1H and ^{13}C NMR chemical shifts and signal assignments for ZnTLMA, TLMA, $ZnBLMA_2$, and $BLMA_2$, ^1H NMR chemical shifts of nonexchangeable protons at different pH values and temperatures for ZnTLMA, ^1H NMR chemical shifts of exchangeable protons, NOEs for ZnTLMA and M−BLMs, Zn−N bond distances and some hydrogen bond distances, the N−Zn−N bond angles for some ZnTLMA models and X-ray structures of M−BLM analogs, results of MM/MD, the energies for the restrained and unrestrained models, and NMR *R*-factors; and figures of HMBC, HMQC, NOESY at 250 ms, the upfield region of the NOESY at 500 ms, DQFCOSY, part of the aromatic region of the NOESY (in H_2O) spectra of ZnTLMA, the four possible configurations for the sp II ZnTLMA model, superimposition of the ten IRMA structures with the lowest potential energy for the *SS*-sp basket, *SS*-sp I, *SS*-tbp, and *SS*-sp basket dimer models, superimposition of the 10 IRMA structures with the lowest potential energy for the *SS*-sp basket monomer and *SS*-sp basket dimer models (only the core 1 atoms are shown), and back-calculated and experimental NOESY spectra (500 ms) for the *SS*-tbp and *SS*-sp basket dimer ZnTLMA models (31 pages). See any current masthead page for ordering and Internet access instructions.

JA963392B